




Comparison in the performance of EDM and NPMEDM using Al₂O₃ nanopowder as an impurity in DI water dielectric

Amit Kumar¹ · Amitava Mandal¹  · Amit Rai Dixit¹ · Alok Kumar Das¹ · Saroj Kumar¹ · Rachit Ranjan¹

Received: 20 February 2017 / Accepted: 21 November 2018 / Published online: 27 November 2018
© Springer-Verlag London Ltd., part of Springer Nature 2018

Abstract

In this paper, an attempt is made to explore the possibilities of modifying the dielectric by adding alumina (Al₂O₃) nanopowder for improving the machining performances. The performance of newly developed nano powder-mixed electrical discharge machining (NPMEDM) process is compared with conventional EDM. Peak current, gap voltage and pulse-on time are taken as considerable process parameters to investigate material removal rate (MRR), surface roughness (SR), recast layer thickness, surface morphology, surface topography and induced residual stress. It is observed that the nanopowder-mixed dielectric medium gives better surface finish and higher metal removal rate as compared to conventional dielectric. The value of MRR increases from 32.75 to 47 mg/min and surface roughness improves from 2.245 to 1.487 μm. Thereafter, atomic force microscopy (AFM) and field emission scanning electron microscopy (FESEM) investigation of the machined surface reveals that presence of micro-crack, micro-hole and uneven deposition decrease substantially during NPMEDM process. Also, induced tensile residual stress on the machined surface significantly reduces in this modified process. Further, the basic mechanism of these processes are investigated by analysing pulse train discharge waveforms and reveals the better sparking stability of NPMEDM process, which results in the higher MRR and better surface quality.

Keywords NPMEDM · Al₂O₃ nanopowder · Surface integrity · AFM · Residual stress

1 Introduction

Nowadays, EDM is used as a method for machining of the difficult-to-cut materials due to its force- and contact-free

machining characteristic. In this process, material removal takes place by rapid sparking (thermal erosion) between two electrodes. The electrodes are separated by a dielectric to provide insulation [1]. As the distance between electrodes decreases, the intensity of the electric field in between the electrodes increases. At a certain point, it becomes greater than the dielectric strength. As a result, spark is generated between the electrodes and electrical energy gets converted into thermal energy. This thermal energy allows melting of material from both the electrodes and are flushed out with the help of a flushing pump. Although EDM process is a potential manufacturing process, its poor surface qualities and material removal rate are considered as the key problems in its development. In order to improve the process, researchers have studied the influence of different parameters and use of various dielectric fluids on its performance. Though the surface roughness of the machined parts by EDM could be controlled by varying the process parameters [2], generation of mirror-finished surface and elimination of other surface defects like micro-crack, micro-holes, craters and uneven deposition of solidified material are the most challenging task. In this regard, powder-mixed EDM process is an emerging method to

✉ Amitava Mandal
amitava03@gmail.com

Amit Kumar
amitkumar158@gmail.com

Amit Rai Dixit
amitraidixit@iitism.ac.in

Alok Kumar Das
alok75@gmail.com

Saroj Kumar
sarojbabu1992@gmail.com

Rachit Ranjan
rachitranjan25@gmail.com

¹ Department of Mechanical Engineering, Indian Institute of Technology (Indian School of Mines), Dhanbad, Jharkhand 826004, India

improve the surface quality of the machined part [3–7]. In the past, many attempts have been made to study the effect of powder-mixed dielectric in EDM by considering different powders like aluminium (Al), carbon (C), copper (Cu) and iron (Fe) [8]. It has been observed that the presence of impurities in the dielectric up to certain percentage improves the machined surface quality whereas the short-circuiting phenomenon may occur at higher powder concentration and it would lead to instability of the process.

Powder-mixed EDM process is an emerging technology where performance parameters are improved by blending powder particles into the dielectric fluid. The powder particles in dielectric increase the presence of number of positive and negative charges between the electrodes. Therefore, in adjacent points of the two particles, intensity of the electrical field becomes more, so the breakdown will occur at these points. Number of particles present in between the discharge gap generates a series of discharge which enlarges the discharge gap. Experimental studies reported that powders in the dielectric increases the electric field intensity and as a result, discharge gap is increased up to three times than conventional EDM process [9]. With the help of this phenomenon, debris particles get easily flushed out, which improves the surface finish and material removal rate (MRR). Experiment on powder-mixed EDM with kerosene as a dielectric medium and graphite powder as an impurity shows that MRR can be increased up to 60% and ignition delay time can also be optimised by selecting proper concentration of graphite powder in dielectric [10]. Use of different micro powders like Al, Al_2O_3 , Si, SiC, Gr and W with kerosene were investigated and found suitable for machining superalloys [11–16]. However, it is observed that the density, resistivity, particle size, particles concentration and electrical and thermal conductivity of the powder influences the process performance significantly [17]. Further, at higher particle size, the MRR reduces due to lower electrical discharge and higher possibility of short circuiting. If the powder particle size is greater than the spark gap, the quality of machining efficiency drops drastically [18]. Smaller powder particles have a significant effect on the machining efficiency. Where the particle size is reduced to nano powder-mixed electric discharge machining (NPMEDM) yields mirror surface finish [19].

In the literature, carbon nanotube (CNT)-mixed kerosene are considered as a dielectric to machine NAK80 die steel and it is concluded that the machining efficiency and surface finish improves by 66% and 70%, respectively, as compared to conventional EDM process [20]. Graphite nanopowder-mixed EDM is also used for machining cemented tungsten carbide (WC–Co) by micro-EDM set up and concluded that the semi-conductive graphite powder can generate a defect-free and uniform surface [3, 17]. Further, experimental results using nano powder particles showed better surface integrity on the EDMed surface in NPMEDM [19]. This is due to better

properties of nano powder in comparison to the micro-sized powder particles. Properties such as larger surface area and smaller size generates bridging phenomenon results in lesser chances of settling down.

In this regard, widely used nano powders like CNT, nano-Gr and nano- TiO_2 [21–24] are mixed with dielectric fluid while investigating the performance in NPMEDM but most of these powders are conductive in nature and are costlier. Till now, little attention has been paid in the use of non conductive nano powders like Al_2O_3 nanoparticles although Al_2O_3 micro particles has been found as a suitable impurity for mixing with dielectric in powder-mixed EDM process [11]. Therefore, Al_2O_3 nanopowder, which has a low density, moderate thermal conductivity, high wear and corrosion resistance properties and cost-effective in comparison to CNTs, is considered in the present study. Further, influence of Al_2O_3 nanoparticles has been studied by mixing with deionised water, which is considered as an appropriate dielectric medium to obtain better surface quality [11]. Moreover, inadequate literature on detailed study into the surface integrity of the machined surface by NPMEDM process attracts the attention of the researchers. Therefore, in this study, all the important aspects of surface integrity like surface topography, surface morphology, recast layer thickness and residual stress present have been investigated. Finally, the basic mechanics of the NPMEDM process is explained by using captured pulse train discharge waveforms.

2 Experimentation

In the present work, experiments are performed on a SPARKONIX ZNC/ENC35 EDM machine (Fig. 1). A tank is used to ensure the effective utilisation of dielectric and dielectric fluid is removed by a pump provided. Here, a servo mechanism provides up and down movements to the electrode tool by keeping a minimum desirable gap between the electrode tool and workpiece. With the application of voltage, the intensity of the electric field becomes higher and exceeds the strength of dielectric which leads to ionisation of the dielectric fluid present between the electrodes in a discreet form. To maintain a constant flow of current between the electrodes, some of the current is bypassed and it is termed as bypass current. Due to this spark generation, the material is removed from both the electrodes.

In this study, the workpiece material is made of Inconel 825 (chemical compositions is presented in Table 1) and copper is taken as tool material and three process parameters namely pulse on time (T_{ON}), peak current (IP), and gap voltage (GV) are considered. The levels with arrangement of these process parameters are presented in Table 2. Response surface methodology (RSM) technique based on Box-Behnken method is used to design the experiment. Total of 15 combinations

Fig. 1 Experimental setup



1 Work piece 2 Tool 3 Tool holder 4 Fixture 5 Flushing pump 6 Oscilloscope 7 Servo controller 8 Control panel

(Table 3) are used to carry out the experiments for both conventional EDM and NPMEDM. The experimental matrix is used to conduct two sets of experiments. In the first set, the deionised water is taken as a dielectric medium. While, in the second set, 1% by weight of Al₂O₃ nanopowder mixed with 1-L deionised water is used. The average particle size of Al₂O₃ nanopowder is 45–50 nm. The prepared deionised water solution is milky white in colour. In both sets of the experiment, other machining parameters (duty cycle 50%, spark timing 3 μs, bypass current 1 A, sensitivity 50% and tool surface area 75 mm²) are kept constant.

During the experimentation, the difference between initial and final weight of the workpiece are noted down along with the machining time (Table 3). Thereafter, MRR is calculated using Eq. 1.

$$MRR = \frac{(W_i - W_f)}{t} \tag{1}$$

where

W_i and W_f = initial and final weight of the workpiece in milligrams, respectively.

Table 1 Chemical composition of workpiece material (in weight %)

Fe	Cu	Al	S	Ti	Co	Ni	Mo	W	Cr
27.1	1.77	0.15	0.03	1.04	0.39	43.75	3.36	0.34	22.12

t = machining time in minutes.

Average surface roughness (SR) of the machined part is measured using SURFTTEST SJ-210 by taking sampling length as 0.8 mm with measuring speed of 0.5 mm/s (Table 3).

3 Response surface modelling

In RSM modelling, relationship between response and process parameters are represented by a quadratic Eq. 2.

$$Y = b_0 + \sum_{i=1}^k b_i X_i + \sum_{i=1}^k b_{ii} X_i^2 + \sum_{j>1}^k b_{ij} X_i X_j \tag{2}$$

where

Y = output response.

x₁, x₂, x₃, ..., x_k = independent variables.

k = number of independent variables.

b₀, b_i, b_{ii}, b_{ij} = coefficients of the equation terms.

Table 2 Machining parameters with their levels

Levels	Peak current Ip (A)	Pulse on time T _{ON} (μs)	Gap voltage, GV (V)
-1	2	8	10
0	5	14	30
+1	8	20	50

Table 3 Experimental matrix

S. No	Process parameters			Response parameters			
	IP (A)	T _{ON} (μs)	GV (V)	MRR _{conv} (mg/min)	SR _{conv} (μm)	MRR _p (mg/min)	SR _p (μm)
1	2	4	30	3.8350	2.5232	6.333	1.4870
2	8	4	30	14.6670	3.1730	18.667	2.7244
3	2	10	30	7.5100	2.7572	6.500	1.6910
4	8	10	30	15.6670	3.2400	37.000	2.8110
5	2	7	10	8.2240	2.3148	8.500	1.8560
6	8	7	10	20.6670	2.7400	36.667	2.8198
7	2	7	50	7.3300	2.4944	8.500	1.8670
8	8	7	50	15.0000	3.4108	22.000	3.3886
9	5	4	10	15.0030	2.4734	19.548	2.1888
10	5	10	10	14.0000	2.7204	31.000	2.4002
11	5	4	50	8.6670	2.8210	8.000	2.5356
12	5	10	50	10.9270	2.8368	15.782	2.8298
13	5	7	30	11.3330	3.3600	18.667	2.5755
14	5	7	30	12.3330	3.2838	17.667	2.5200
15	5	7	30	12.6670	3.2200	16.667	2.5600

Using MINITAB 17 statistical software package, regression models of MRR and SR are developed based on the generated experimental data. The developed models are presented by Eqs. 3, 4, 5, and 6, respectively.

$$MRR_{conv} = 12.111 + 7.084 Ip + 2.331 TON - 4.433 GV + 0.571 Ip \times Ip - 0.826 TON \times TON + 2.456 GV \times GV + 1.391 Ip \times TON - 3.527 Ip \times GV + 0.022 TON \times GV \quad (3)$$

$$SR_{conv} = 3.2879 + 0.3093 Ip + 0.0705 TON + 0.1643 GV - 0.1687 Ip \times Ip - 0.1958 TON \times TON - 0.3792 GV \times GV - 0.0417 Ip \times TON + 0.1228 Ip \times GV - 0.0578 TON \times GV \quad (4)$$

Table 4 Analysis of variance for MRR_{conv}

Source	DF	Seq SS	Adj SS	Adj MS	F	P VALUE
Regression	9	686.493	686.493	76.277	98.49	0
Linear	3	602.141	602.141	200.714	259.16	0
Square	3	26.869	26.869	8.956	11.56	0.011
Interaction	3	57.484	57.484	19.161	24.74	0.002
Residual error	5	3.872	3.872	0.774		
Lack-of-fit	3	2.909	2.909	0.97	2.01	0.349
Pure error	2	0.964	0.964	0.482		
Total	14	690.366				
S = 0.880046	Press = 48.7075					
R ² = 99.44%	R ² (pred) = 92.94			R ² (adj) = 98.43%		

$$MRR_{NPMEDM} = 17.67 + 10.563 Ip + 4.717 TON - 5.179 GV - 0.10 Ip \times Ip - 0.44 TON \times TON + 1.35 GV \times GV + 4.54 Ip \times TON - 3.67 Ip \times GV - 0.92 TON \times GV \quad (5)$$

$$SR_{NPMEDM} = 2.5518 + 0.6053 Ip + 0.0995 TON + 0.1695 GV - 0.1896 Ip \times Ip - 0.1839 TON \times TON + 0.1206 GV \times GV - 0.0294 Ip \times TON + 0.1395 Ip \times GV + 0.0207 TON \times GV \quad (6)$$

Further, ANOVA analysis of these four models are carried out at 95% confidence level. Higher F value in ANOVA table indicates the significant effect of process parameters (Tables 4, 5, 6, 7). The values of R² and adjusted R² of all the developed models for MRR are found to be above 98% and 96% for conventional EDM and NPMEDM, respectively. Similarly, the value of R² and adjusted R² of all the developed models for SR are found to be above 94% and 98% for conventional EDM and NPMEDM, respectively.

To find the optimal combinations of process parameters, the desirability function approach is used. The individual response Y_i is transformed into desirability function D_i(Y_i) for possible value of Y_i [25].

$$D_i(Y_i) = \begin{cases} 0 & \text{for completely undesirable value of } y_i \\ 1 & \text{for completely desirable value of } y_i \end{cases} \quad (7)$$

Using MINITAB 17, maximum MRR of 34 mg/min and 48.063 mg/min are predicted by the optimal setting of IP at 8 Amp, T_{ON} at 20 μs and GV at 10 V for conventional EDM and NPMEDM, respectively. To validate the predicted values, experiments are conducted and found MRR of 32.75 mg/min and 47 mg/min for conventional EDM and NPMEDM, respectively, which indeed is in better agreement with the predicted values. Similarly, minimum SR of 2.0234 μm and 1.444 μm are predicted for conventional EDM and NPMEDM, respectively, by setting of process parameters at IP 2 Amp, T_{ON} 8 μs

Table 5 Analysis of variance for MRR_p

Source	DF	Seq SS	Adj SS	Adj MS	F	P value
Regression	9	1432.73	1432.73	159.193	38.76	0
Linear	3	1285.12	1285.12	428.374	104.3	0
Square	3	7.96	7.96	2.655	0.65	0.618
Interaction	3	139.65	139.65	46.549	11.33	0.011
Residual error	5	20.54	20.54	4.107		
Lack-of-fit	3	18.54	18.54	6.179	6.18	0.142
Pure error	2	2	2	1		
Total	14	1453.27				
S = 2.02661	Press = 301.073					
R ² = 98.59%	R ² (pred) = 79.28			R ² (adj) = 96.04%		

and GV 30 V. From the validation result, the values of SR in conventional EDM and NPMEDM are found as 2.245 μm and 1.487 μm, which are close to the predicted values.

4 Improvement in process performance of NPMEDM over conventional EDM

The effect of process parameters on the responses are investigated for both set of experiments. The influence of process parameters on MRR and SR are plotted (Figs. 2a–d and 3a–d). Considering optimum machining conditions for minimum surface roughness during conventional EDM and NPMEDM processes, improvement in surface morphology, surface topography, and recast layer are investigated using captured FESEM and AFM images (Figs. 4 and 5). Also, investigation into other surface integrity properties of the generated surfaces are carried out in the subsequent sub-sections.

4.1 Improvement in MRR

The MRR in EDM process mainly reflect the machining efficiency. Therefore, it is considered as one of the important

performance measure during machining. Using Eqs. 3 and 5, different graphs (Fig. 2a–d) are plotted to investigate the effects of process parameters on MRR in both the cases. Figure 2a reveals the influence of IP on MRR at different values of T_{ON} by considering GV as constant. It is observed that MRR is maximum for higher IP and T_{ON} due to the longer spark duration with larger energy, which leads to higher melting of the materials. Similarly, Fig. 2b indicates the effects of IP on MRR at various GV by taking T_{ON} as constant. Higher MRR is observed at lower values of GV because lower GV causes intense spark between the workpiece and tool electrodes with maximum discharge efficiency [25]. However, MRR is always higher in NPMEDM as compared to conventional EDM. This may be due to generation of series of sparks in the powder-mixed EDM process. This phenomenon increases the material melting and yields in increased MRR. Also, this process is assisted in widening of electrode gap, which provides better flushing conditions for removal of the melted material [3, 19].

4.2 Improvement in SR

Process parameters’ influence on SR is examined by Fig. 3a–d. Figure 3a illustrates the effect of IP on SR by

Table 6 Analysis of variance for SR_{conv}

Source	DF	Seq SS	Adj SS	Adj MS	F	P value
Regression	9	1.79649	1.79649	0.19961	29.24	0.001
Linear	3	1.0209	1.0209	0.340299	49.85	0
Square	3	0.69494	0.69494	0.231645	33.93	0.001
Interaction	3	0.08065	0.08065	0.026885	3.94	0.087
Residual error	5	0.03413	0.03413	0.006826		
Lack-of-fit	3	0.02431	0.02431	0.008102	1.65	0.399
Pure error	2	0.00983	0.00983	0.004913		
Total	14	1.83062				
S = 0.0826212	Press = 0.410998					
R ² = 98.14%	R ² (pred) = 77.55%			R ² (adj) = 94.78%		

Table 7 Analysis of variance for SR_p

Source	DF	Seq SS	Adj SS	Adj MS	F	P Value
Regression	9	3.64382	3.64382	0.40487	141.68	0
Linear	3	3.24067	3.24067	1.08022	378	0
Square	3	0.32019	0.32019	0.10673	37.35	0.001
Interaction	3	0.08296	0.08296	0.02765	9.68	0.016
Residual error	5	0.01429	0.01429	0.00286		
Lack-of-fit	3	0.01265	0.01265	0.00422	5.14	0.167
Pure error	2	0.00164	0.00164	0.00082		
Total	14	3.65811				
$S = 0.0534575$		Press = 0.206064				
$R^2 = 99.61\%$		R^2 (pred) = 94.37%		R^2 (adj) = 98.91%		

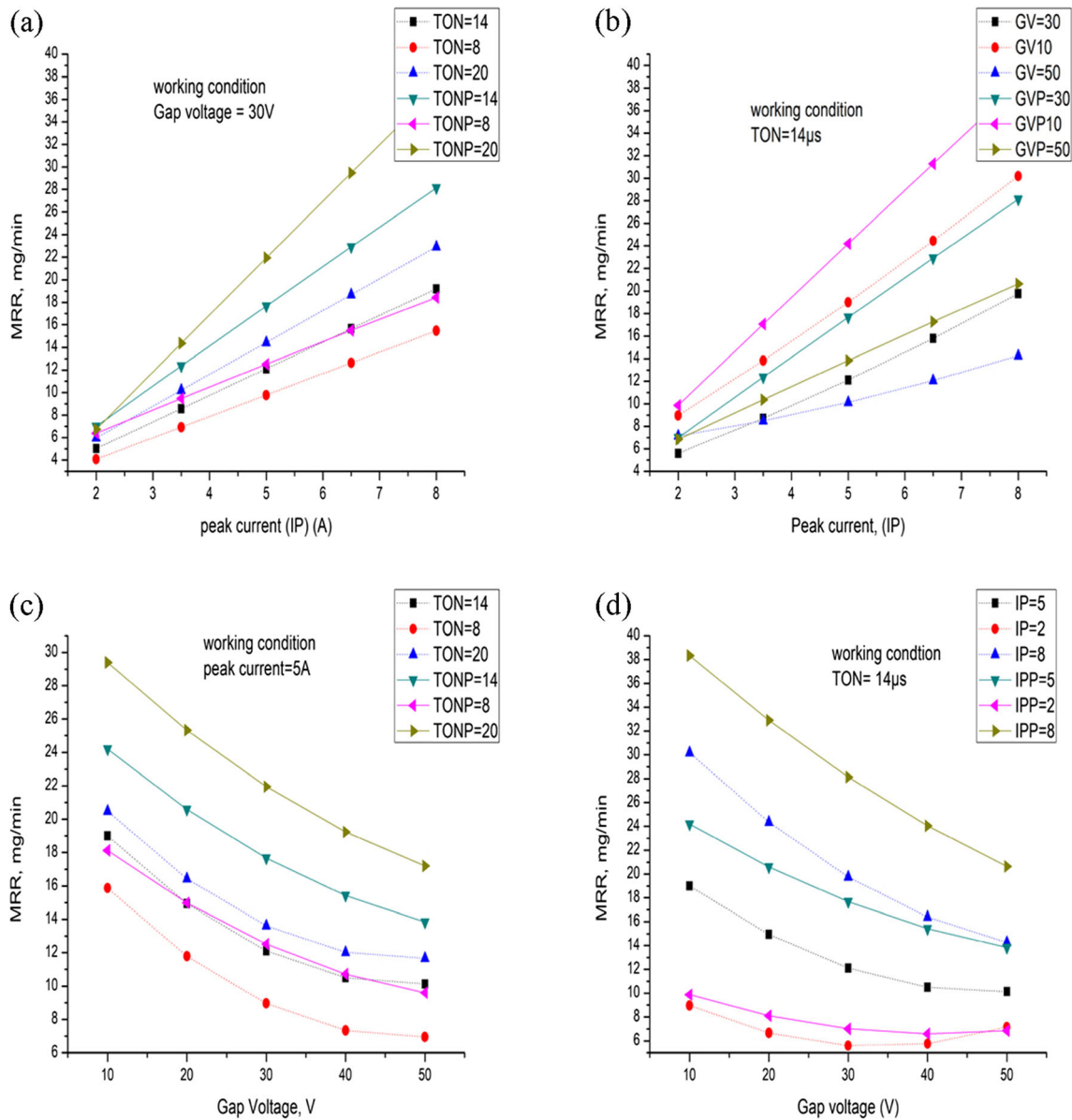


Fig. 2 Effect of peak current on the MRR **a** at various T_{ON} and **b** at various GV. Effect of gap voltage on the MRR **c** at various T_{ON} and **d** at various IP

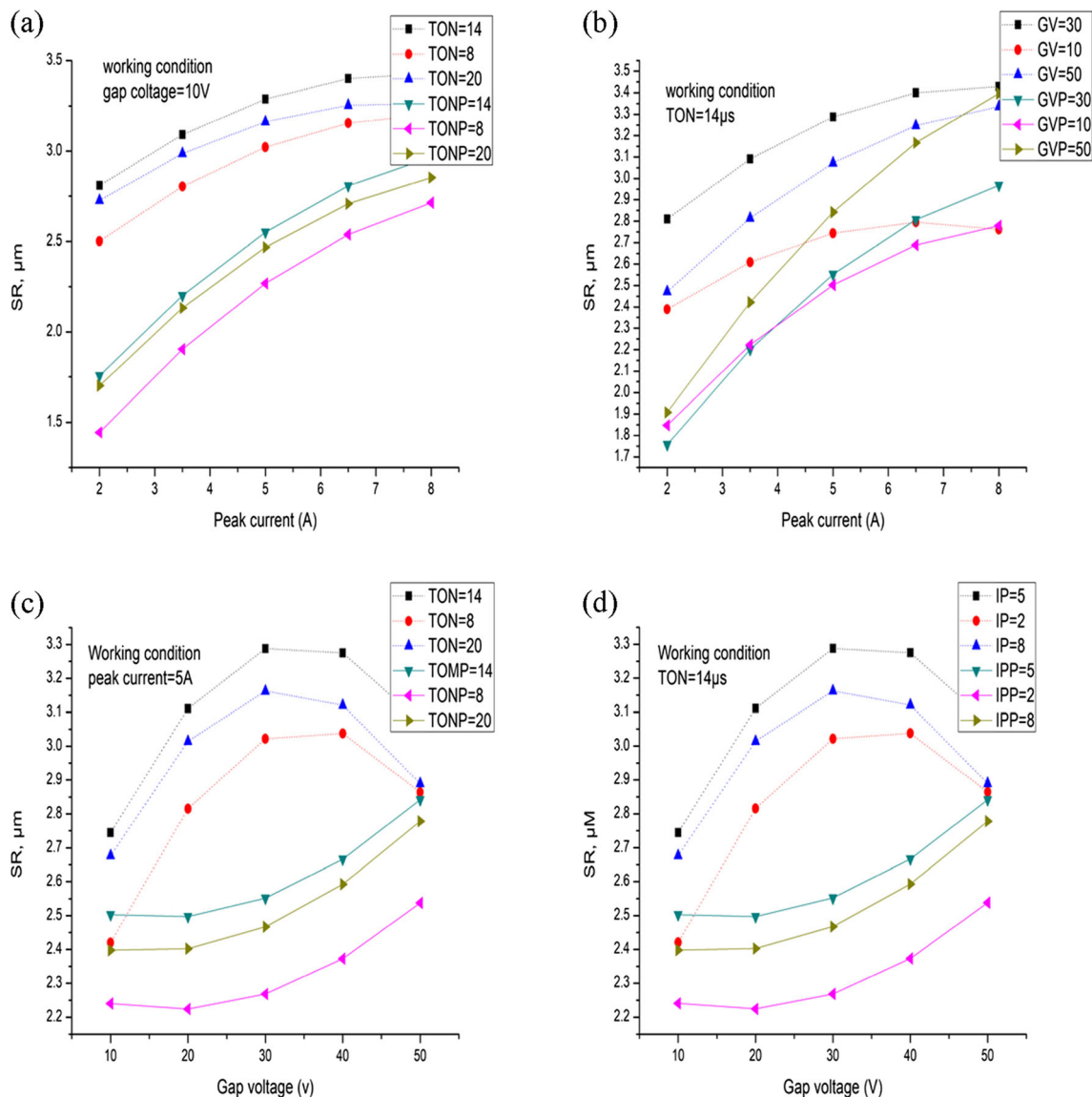


Fig. 3 Effect of peak current on the SR **a** at various T_{ON} and **b** at various GV. Effect of gap voltage on the SR **c** various T_{ON} and **d** at various IP

keeping GV constant at 30 V for varying T_{ON} . It is observed that SR increases as the IP is increased and correspondingly surface finish improves when T_{ON} is decreased. Smoothest surface may be obtained at lowest IP of 2A and T_{ON} of 8 μ s because of lower pulse energy. From Fig. 3a–d, in the beginning, the SR value increases with some certain values of IP, GV, and T_{ON} then it starts to decline for both conventional and NPMEDM process. This trend is found due to the unstable machining conditions and short circuiting beyond these certain values of the process parameters. However, the SR is always higher in conventional EDM as compared to NPMEDM. This observed higher values of SR in plain deionised water is may be due to short-circuiting at lower gap between the electrodes [3].

4.3 Improvement in surface morphology and topography

Surface morphology and topography are investigated using FESEM images at different magnification are shown in Fig. 4a, b. For conventional EDM (Fig. 4a), it is observed that there are numbers of micro holes, cracks, non-uniform solidified metal deposition, and improper machining marks. These undesirable phenomena may be due to intense sparking at the smaller gap in conventional EDM process. However, in the powder-mixed EDM, a uniform sparking takes place at a higher gap between the electrodes which allows easy removal of debris particles. Figure 4b shows the surface morphology generated by NPMEDM and it is clear from the FESEM

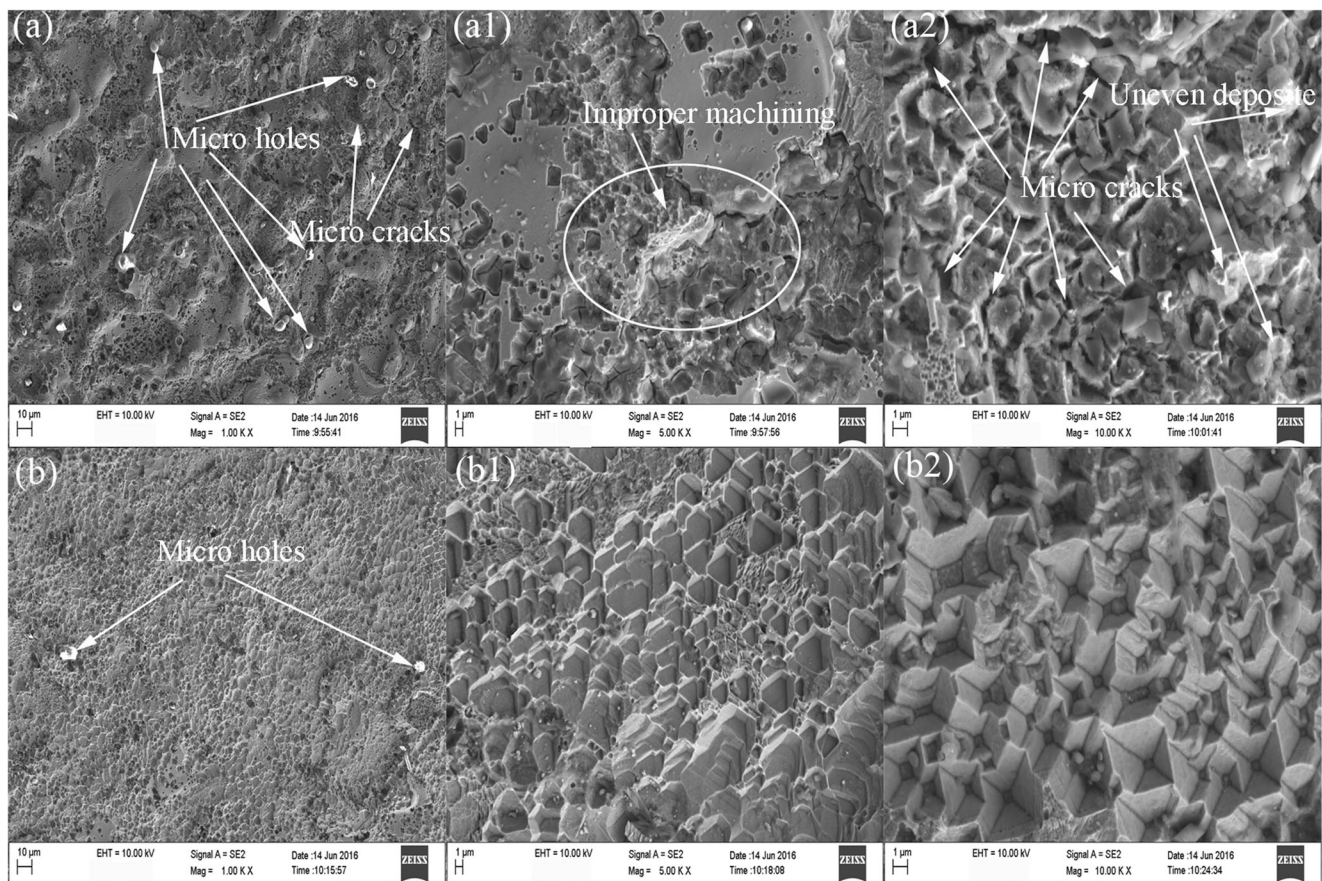


Fig. 4 Surface morphology obtained from conventional EDM **a** at 1-kx magnification, **a1** at 5-kx magnification and **a2** at 10-kx magnification and from NPMEDM **b** at 1-kx magnification, **b1** at 5-kx magnification and **b2** at 10-kx magnification

images that these undesirable phenomena are comparatively less on the generated surface. Also, at a higher magnification, hexagonal-shaped craters (Fig. 4b2) are observed on the machined surface as melted material in each spark flushed out completely leaving the crater marks. Whereas, in the case of conventional EDM process, irregular deposition of re-

solidified material with number of micro-cracks (Fig. 4a2) are observed.

Further, atomic force microscopy (AFM) analysis is also carried out to investigate the surface topography of the machined surfaces. The images of the samples generated by EDM and NPMEDM are taken by AFM machine

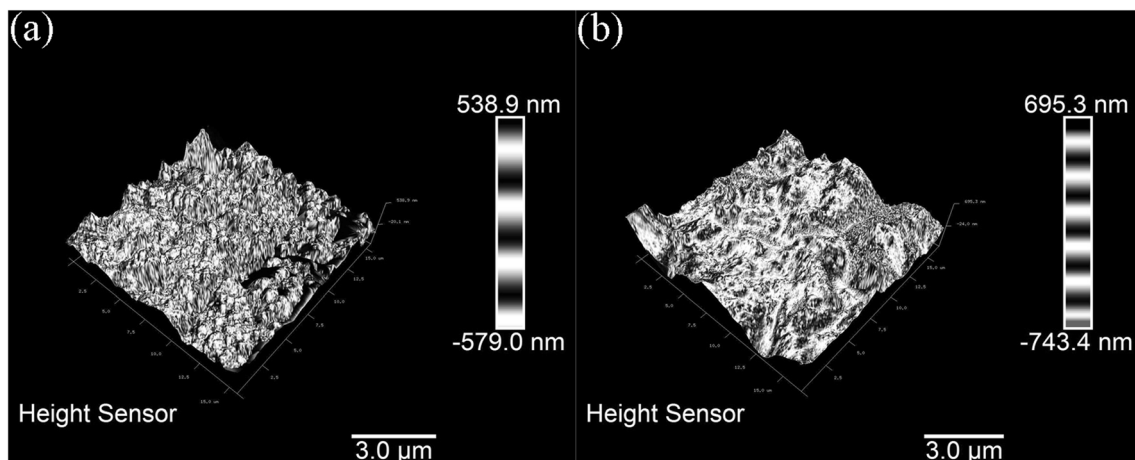


Fig. 5 3-D AFM images of 15 μm × 15 μm scan size for **a** NPMEDM and **b** conventional EDM.

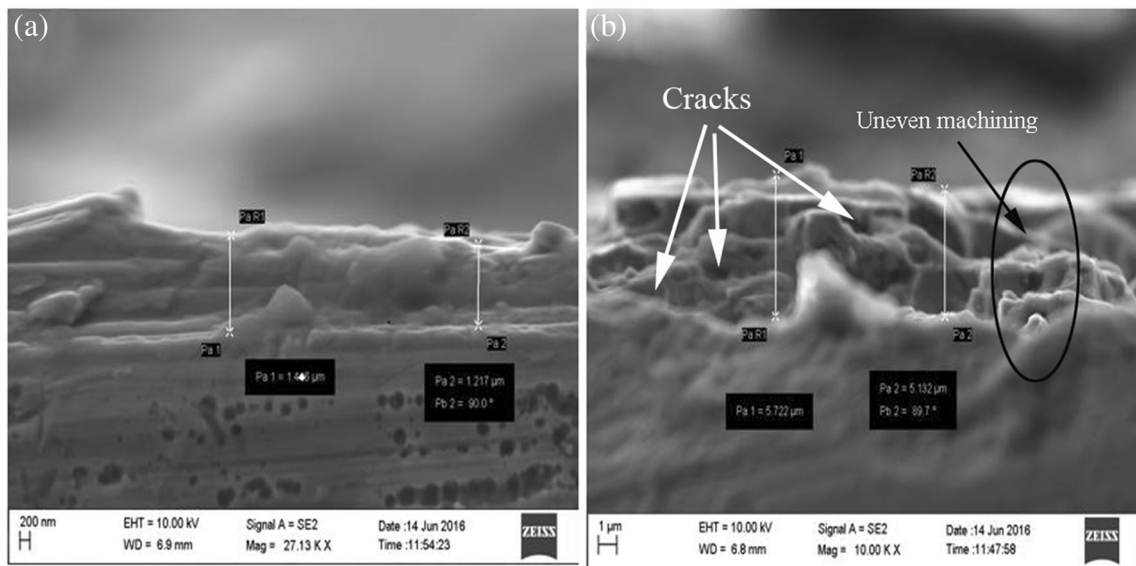


Fig. 6 Recast layer thickness in a NPMEDM and b conventional EDM

(Dimension Icon, Bruker); for tapping, RTESPA probe is used. The length, width and thickness of the cantilever are taken as 125 μm, 35 μm and 3.75 μm, respectively. The oscillation frequency and spring constant are fixed at 300 kHz and 40 N/m, respectively, with the scan size as 15 μm × 15 μm. The captured images of the surface topography with height mapping bar for both the process are shown in Fig. 5a, b. From the captured images, it can be concluded that the surface topography, in the case of conventional EDM, is more irregular as compared to NPMEDM. The graphs show that the distances between peaks to valleys of the surface are in the range of 1.4 μm (Z height from -743.4 to 695.3 nm) and 1.1 μm (Z height from -579.0 to 538.9 nm) in conventional EDM and NPMEDM, respectively. Moreover, it is shown in Fig. 5 that the waviness of the surface, obtained by conventional process, is higher in comparison to the NPMEDM.

These observed phenomena in NPMEDM process are supported by the past literature [26].

4.4 Improvement in deposition of recast layer

Recast layer is the deposition of re-solidified metal (undesirable phenomenon) over the surface of the workpiece. Recast layer thickness is examined by cutting the sample in transverse direction into two parts using wire-EDM and then samples are polished up to mirror finish condition. Thereafter, etchant is applied over the surface. FE-SEM (Supra 55) is used to analyse the subsurface characteristics (Fig. 6). From the analysis, it is observed that the thickness of the recast layer are 5–6 μm and 1–2 μm in conventional EDM and NPMEDM, respectively. It may be due to increased electrode gap distance which

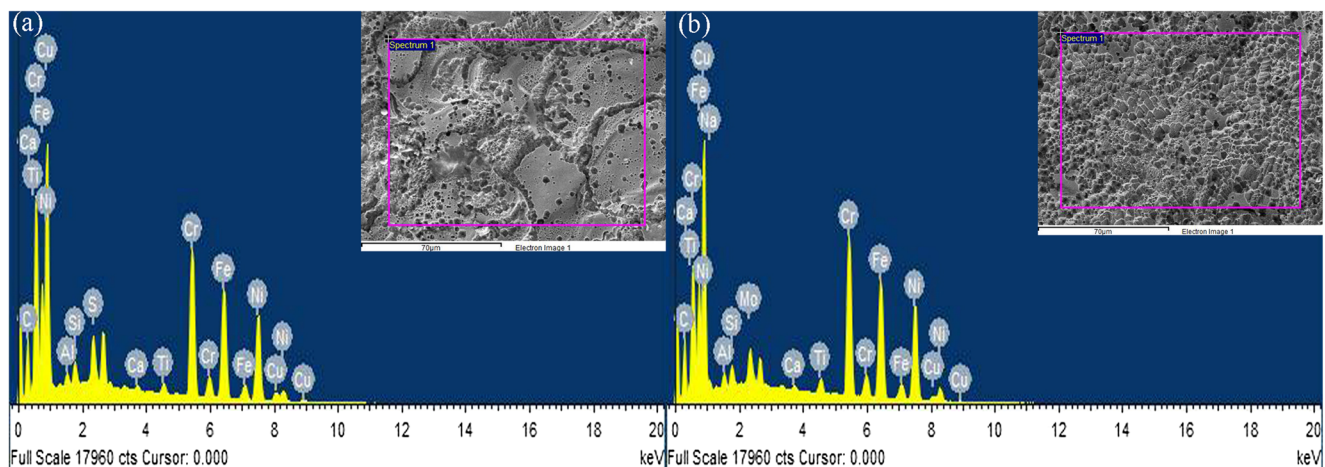


Fig. 7 EDS of machined surface a conventional EDM and b NPMEDM

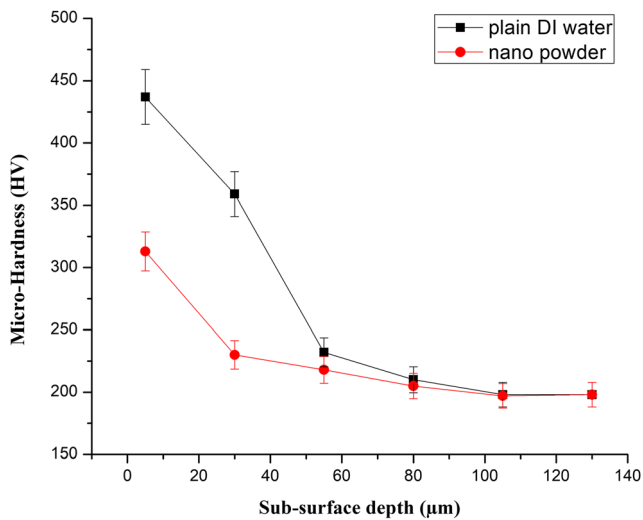
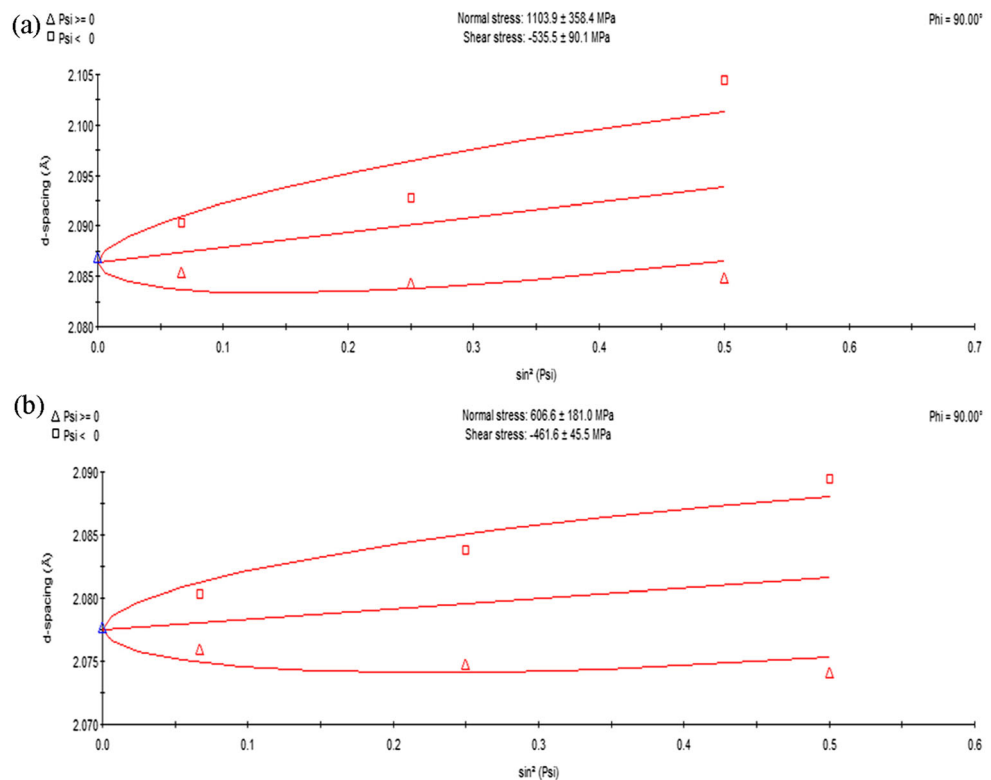


Fig. 8 Sub-surface micro-hardness profiles

improves the flushing condition. As a result, melted material gets less chances to redeposit on the machined surface. Also, in conventional EDM process, the sample shows recast layer with non-uniform deposition. Further, EDS (energy-dispersive x-ray spectroscopy) analysis of machined surface (Fig. 7) shows that there is no transfer of alumina powder, external elements and electrode materials on the machined surface.

Fig. 9 d -spacing – $\sin^2\psi$ graph at a plain EDM and b NPMEDM



4.5 Improvement in sub-surface micro-hardness

The micro-hardness of the transversely cut samples' subsurface layers are measured by microhardness measuring machine (Chennai metco VH-01) with 10-s dwell time and 100-g load capacity. The first measurement is taken near to the recast layer, thereafter, measurement is taken at a distance of 25 μm from the initial point as shown in Fig. 8. Results show that the micro-hardness at the recast layer is found to be higher when compared to the base metal due to the surface quenching phenomenon caused by high-energy spark resulted from small gaps present between the tool and work piece. Near the recast layer, the values of micro-hardness are 480 HV and 350 HV for sample obtained from conventional EDM and NPMEDM, respectively. In the case of NPMEDM, there is a possibility of lesser quenching effects as discharge sparks in this process are lower and distributed. However, away from the recast layer, the micro-hardness values reduce drastically and converge with the hardness property of the base material.

4.6 Improvement in induced tensile residual stress

Tensile nature of residual stresses are induced on the generated surface in the EDM process due to the rapid cooling of the material after each spark. When these

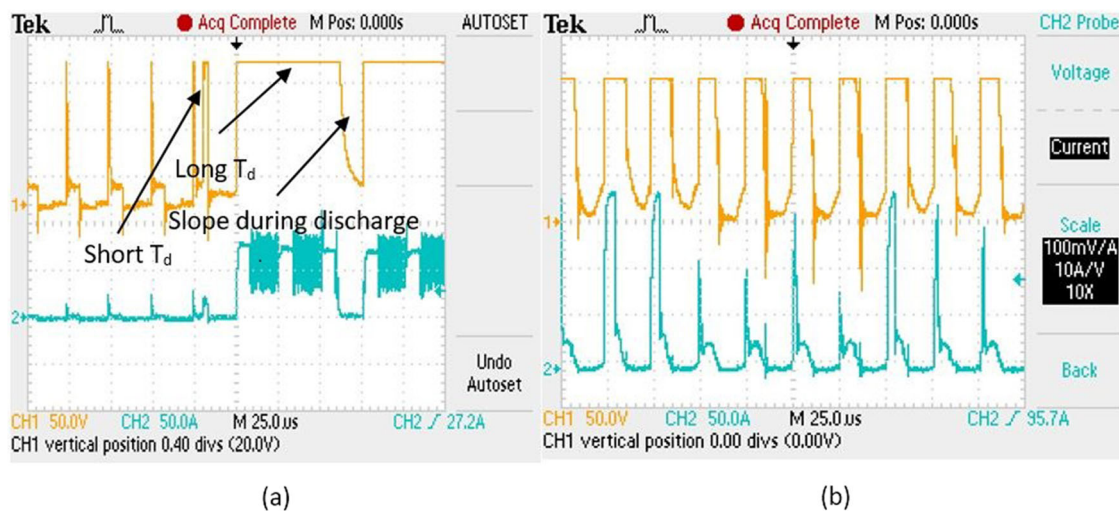


Fig. 10 Pulse train waveform during **a** conventional EDM and **b** NPMEDM

stresses exceeds the fracture strength of that material, cracks formation on the surface may take place. Therefore, the tensile nature of stress present in the material is more harmful. So, it is necessary to investigate the residual stresses of the machined surface obtained by EDM processes. In this regard, XRD analysis is carried out to measure the induced residual stresses on the machined surface.

Crystal is a periodic arrangement of atoms in all the directions but due to induced residual stresses, these atoms are distorted. This change from the perfect crystal gives some peak which is known as diffraction peak. Using these peaks, many important properties like crystal size, lattice strain, and residual stress can be estimated. In this study, X'Pert PRO XRD machine is used (made in Netherlands) to measure diffraction pattern and thereafter diffraction peaks are located. In this process, copper is used to produce x-rays at 40 kV and 30 mA with a wavelength of 1.54056 Å. Using X'pert stress software, the induced residual stresses are calculated and the slope is found to be 1.234E-02 and 7.781E-03 (Fig. 9a, b) for conventional EDM and NPMEDM, respectively. Further, the range of tensile stresses are measured in conventional and nano powder-mixed EDM are 745.5 to 1462.3 MPA (1103.9 ± 358.4 MPA) and 425.6 to 787.6 MPA (606.6 ± 181.0 MPA), respectively. It is observed that the induced residual stresses are much higher in the generated surface by conventional EDM as compared to NPMEDM. The reason for this improvement in NPMEDM may be due to low discharge energy density spark at a higher gap between the electrodes. The minimum value of the tensile stress is measured in powder mixed EDM process and the value is 425.6 MPA which makes the component safe to use in the industrial applications.

5 Mechanism

The experimental study shows that the NPMEDM process consists of different mechanism from that of conventional EDM, which improves the MRR and surface integrity. Theoretical investigation shows that the suspended particles in the dielectric fluid may impact the machining parameters and can be controlled by decreasing the time lag. Hence, to understand the mechanism of NPMEDM process and conventional EDM, the discharge waveforms are recorded and examined (Fig. 8). The selected process parameters are 8 amp (IP), 20 μs (T_{ON}) and 30 volts (GV). It is found that the ignition delay time (T_d), which plays crucial role by providing insulation and resting period between the electrode gaps, is very irregular in conventional EDM (Fig. 10a). Thus, all the phenomena like short T_d , long T_d , very short T_d or arcing as well as slope during discharge are visible. While for nano powder-mixed EDM, the normal ignition delay time (T_d) and waveforms are shown in Fig. 10b. Abnormal discharge waveforms generated in conventional EDM may be because of the presence of particles debris in the gap. However, in NPMEDM, the gap between the electrodes increases. As a result, proper sweeping can be provided to reduce the chance of arcing. Further, surface integrity improvement by NPMEDM process is due to evenly distributed and shallow-shaped etched cavities on the surface with same discharge energy when compared to conventional EDM.

6 Conclusions

In the present investigation, the conventional EDM process is modified by replacing EDM oil with Al_2O_3 nanopowder mixed deionised water. The machining performance is analysed on

Inconel 825 superalloy, which is widely used in the nuclear power plant, petrochemical, chemical, missile industries and highly corrosive environment. The relationship between process parameters and responses are established using RSM model. A detailed investigation on surface integrity of the machined parts are conducted using FESEM, AFM, EDS and XRD. Based on the experimental results analysis following conclusions are drawn:

1. Al_2O_3 nanoparticle, which is a non-conductive powder, mixed with deionised water is found efficient in terms of MRR, surface finish and surface integrity parameters for machining of Inconel 825 in NPMEDM process.
2. Both MRR and SR are improved in NPMEDM process due to the widening of the electrode gap, uniform sparking and no arcing condition of nanoparticles between the electrodes.
3. In this modified process, increment in MRR up to 57% is achieved and average surface roughness of the generated surface is restricted by $1.487 \mu\text{m}$, which is 63% less compared to conventional EDM.
4. Due to the proper flushing of the debris particles from the machining zone, re-deposition of the solidified material is diminished and therefore, the hexagonal shaped cavities are observed on the surface generated by NPMEDM. Whereas, on the surface generated by conventional EDM, lot of micro-holes, micro-cracks and irregular deposition of solidified materials are observed.
5. The observed thickness of recast layer during NPMEDM is in the range of 1 to $2 \mu\text{m}$, which is almost one third of the observed recast layer thickness during conventional EDM.
6. At the re-solidified layer, hardness of the material increases drastically due to quenching phenomenon. However, the observed micro-hardness on the recast layer during NPMEDM is quite lower in comparison to conventional EDM.
7. Higher discharge energy yields higher residual stresses and therefore, the observed tensile residual stresses on the generated surface by conventional EDM are 1103.9 ± 358.4 . Whereas the same in NPMEDM are found to be 606.6 ± 181.0 MPA.
8. Verified by the obtained pulse train waveforms, less problem of short circuiting is observed in NPMEDM as compared to conventional EDM. This may be due to the larger gap size between the electrodes in NPMEDM which decreases the chances of debris particles' presence between the electrodes.

Acknowledgements This paper is a revised and expanded version of the paper entitled "Comparison of Surface Roughness and Material Removal Rate in Die Sink EDM using Deionized Water and Powder Mixed DI water as a Dielectric Medium" presented at 6th International & 27th All India Manufacturing Technology, Design and Research Conference (AIMTDR2016), College of Engineering Pune, India, December 16–18, 2016.

Publisher's Note Springer Nature remains neutral with regard to jurisdictional claims in published maps and institutional affiliations.

References

1. Zhao WS, Meng QG, Wang ZL (2002) The application of research on powder mixed EDM in rough machining. *J Mater Process Technol* 129:30–33
2. Kiyak M, Çakir O (2007) Examination of machining parameters on surface roughness in EDM of tool steel. *J Mater Process Technol* 191:141–144. <https://doi.org/10.1016/j.jmatprotec.2007.03.008>
3. Baseri H, Sadeghian S (2016) Effects of nanopowder TiO_2 -mixed dielectric and rotary tool on EDM. *Int J Adv Manuf Technol* 83: 519–528
4. Patel S, Thesiya D, Rajurkar A (2018) Aluminium powder mixed rotary electric discharge machining (PMEDM) on Inconel 718. *Aust J Mech Eng* 16:21–30. <https://doi.org/10.1080/14484846.2017.1294230>
5. Kumar VS, Kumar PM (2015) Machining process parameter and surface integrity in conventional EDM and cryogenic EDM of Al-SiCp MMC. *J Manuf Process* 20:70–78. <https://doi.org/10.1016/j.jmapro.2015.07.007>
6. Bajpai V, Mahabare P, Singh RK (2016) Effect of thermal and material anisotropy of pyrolytic carbon in vibration-assisted micro-EDM process. *Mater Manuf Process* 31:1879–1888. <https://doi.org/10.1080/10426914.2015.1127937>
7. Singh R (2010) Characterization of micro-EDM process for pyrolytic. Carbon 2010–2013
8. Erden A, Bilgin S (1981) Role of impurities in electric discharge machining. In: Proceedings of the twenty-first international machine tool design and research conference. Springer, pp 345–350
9. Kozak J, Rozenek M, Dabrowski L (2003) Study of electrical discharge machining using powder-suspended working media. *Proc Inst Mech Eng Part B J Eng Manuf* 217:1597–1602
10. Jeswani ML (1981) Effect of the addition of graphite powder to kerosene used as the dielectric fluid in electrical discharge machining. *Wear* 70:133–139. [https://doi.org/10.1016/0043-1648\(81\)90148-4](https://doi.org/10.1016/0043-1648(81)90148-4)
11. Assarzadeh S, Ghoreishi M (2013) A dual response surface-desirability approach to process modeling and optimization of Al_2O_3 powder-mixed electrical discharge machining (PMEDM) parameters. *Int J Adv Manuf Technol* 64:1459–1477. <https://doi.org/10.1007/s00170-012-4115-2>
12. Peças P, Henriques E (2008) Effect of the powder concentration and dielectric flow in the surface morphology in electrical discharge machining with powder-mixed dielectric (PMD-EDM). *Int J Adv Manuf Technol* 37:1120–1132
13. Singh AK, Kumar S, Singh VP (2015) Effect of the addition of conductive powder in dielectric on the surface properties of superalloy super co 605 by EDM process. *Int J Adv Manuf Technol* 77: 99–106. <https://doi.org/10.1007/s00170-014-6433-z>
14. Prihandana GS, Mahardika M, Hamdi M, Wong YS, Mitsui K (2011) Accuracy improvement in nanographite powder-suspended dielectric fluid for micro-electrical discharge machining processes. *Int J Adv Manuf Technol* 56:143–149
15. Bhattacharya A, Batish A, Singh G, Singla VK (2012) Optimal parameter settings for rough and finish machining of die steels in powder-mixed EDM. *Int J Adv Manuf Technol* 61:537–548
16. Bhattacharya A, Batish A, Kumar N (2013) Surface characterization and material migration during surface modification of die steels with silicon, graphite and tungsten powder in EDM process. *J Mech Sci Technol* 27:133–140
17. Jahan MP, Rahman M, Wong YS (2011) Study on the nano-powder-mixed sinking and milling micro-EDM of WC-Co. *Int*

- J Adv Manuf Technol 53:167–180. <https://doi.org/10.1007/s00170-010-2826-9>
18. Tzeng Y-F, Lee C-Y (2001) Effects of powder characteristics on electrodischarge machining efficiency. *Int J Adv Manuf Technol* 17:586–592
 19. Kumar H (2014) Development of mirror like surface characteristics using nano powder mixed electric discharge machining (NPMEDM). *Int J Adv Manuf Technol* 76:105–113. <https://doi.org/10.1007/s00170-014-5965-6>
 20. Mai C, Hocheng H, Huang S (2012) Advantages of carbon nanotubes in electrical discharge machining. *Int J Adv Manuf Technol* 59:111–117. <https://doi.org/10.1007/s00170-011-3476-2>
 21. Mohal S, Kumar H (2017) Parametric optimization of multiwalled carbon nanotube-assisted electric discharge machining of Al-10%SiC_p metal matrix composite by response surface methodology. *Mater Manuf Process* 32:263–273. <https://doi.org/10.1080/10426914.2016.1140196>
 22. Janmanee P, Muttamara A (2012) Surface modification of tungsten carbide by electrical discharge coating (EDC) using a titanium powder suspension. *Appl Surf Sci* 258:7255–7265
 23. Prabhu S, Vinayagam BK (2010) Analysis of surface characteristics of AISI D2 tool steel material using electric discharge machining process with single wall carbon nano tubes. *Int J Eng Technol* 2:35–41. <https://doi.org/10.7763/IJET.2010.V2.96>
 24. Prabhu S, Vinayagam BK (2013) AFM nano analysis of inconel 825 with single wall carbon nano tube in die sinking EDM process using taguchi analysis. *Arab J Sci Eng*:1–15
 25. Mandal A, Dixit AR, Das AK, Mandal N (2016) Modeling and optimization of machining Nimonic C-263 Superalloy using multicut strategy in WEDM. *Mater Manuf Process* 31:860–868
 26. Guu YH (2005) AFM surface imaging of AISI D2 tool steel machined by the EDM process. *Appl Surf Sci* 242:245–250. <https://doi.org/10.1016/j.apsusc.2004.08.028>